POWER LAWS AND SCALING OF RAIN EVENTS AND DRY SPELLS IN THE CATALONIA REGION

ANNA DELUCA AND ÁLVARO CORRAL

Abstract. We analyze the statistics of rain-event sizes, rain-event durations, and dry-spell durations in a network of 20 rain gauges scattered in an area situated close to the NW Mediterranean coast. Power-law distributions emerge clearly for the dry-spell durations, with an exponent around 1.50 ± 0.05, although for event sizes and durations the power-law ranges are rather limited, in some cases. Deviations from power-law behavior are attributed to finite-size effects. A scaling analysis helps to elucidate the situation, providing support for the existence of scale invariance in these distributions. It is remarkable that rain data of not very high resolution yield findings in agreement with self-organized critical phenomena.

1. Introduction

The concept of self-organized criticality (SOC) aims for explaining the origin of power-law distributed event sizes in a broad variety of systems [1, 2, 3, 4]. Indeed, it has been found that for diverse phenomena that take place in terms of bursts of activity interrupting larger quiet periods, the size s of these bursty episodes or events follows a power-law distribution,

$$P_s(s) \propto \frac{1}{s^{\tau_s}}, \tag{1}$$

over a certain range of s, with $P_s(s)$ the probability density of the event size and τ_s its exponent (and the sign $\propto$ indicating proportionality).

The paradigmatic example of this behavior is a sandpile that is perturbed by the slow addition of extra grains: most of the time the activity in the pile is negligible, but at some instant a new added grain triggers an instability that propagates through the system in the form of an avalanche; these are the high-activity periods whose size is power-law distributed; the avalanche size can be measured from the dissipation of energy, as the change in potential energy before and after the event, for example [5].

Power-law distributions signal the absence of characteristic scales [4, 6]. The main idea behind SOC is the recognition that such scale invariance in event sizes is achieved because of the existence of a nonequilibrium continuous phase transition whose critical point is an attractor of the dynamics [7, 8, 9]. When the system settles at the critical point, scale invariance and power-law behavior is ensured, as these peculiarities are the defining characteristics of critical phenomena [4]. (Notice that from this point of view, SOC is just a suggestion for the origin of scale invariance, other mechanism can lead to the same observable results [3].)

Although the original idea of SOC was inspired mainly by a variety of systems in condensed-matter physics [10], the concept has been particularly fruitful in the geosciences, with a special impact in natural hazards. Indeed, earthquakes [1, 11], landslides and rock avalanches [12], volcanic eruptions [12, 13], forest fires [14], and even the extinction of biological species [15], have been proposed as realizations of SOC systems.

However, the penetration of atmospheric science by SOC has been much more modest. As far as we know, the pioneering papers are those of [16] and Peters et al. [17, 18, 19], who studied rainfall as an avalanche process. Both authors dealt with locally measured precipitation and defined, independently, a rain event as the sequence of rain occurrence for which the rain rate (i.e., the activity) is always greater than zero. Then, the focus of the SOC approach is not on the total amount of rain recorded in a fixed time period (for instance, one day, or one month), but on the rain event, which is what defines in each case the time period of rain-amount integration. In this way, the event size is the total amount of rain collected during the duration of the event. We can recognize a contraposition between the anthropogenic perspective, paying attention to rain over relatively large time periods, and a more physical approach, looking at the fine structure of the rainfall phenomenon [18].

The analysis of Andrade *et al.* considered long-term daily rain records from several weather stations in Brazil, India, Europe, and Australia, with observation times ranging from a dozen years up to more than a century. The rain rate was taking values between 0.1 mm/day to about 100 mm/day. Although the dry spell (the time between rain events) seemed to follow a steep power-law distribution (at least for some stations in semi-arid regions), the rain-event size was not reported, and therefore the possible connection between SOC and rainfall could not be really checked.

On the other hand, Peters *et al.* used in their study a totally different dataset, obtained from the operation of a vertically pointing Doppler radar situated in the Baltic coast of Germany. This facility provided rain rates at an altitude between 250 m and 300 m above sea level, covering an area of 70 m^2, with a detection threshold equal to 0.005 mm/hour at a one-minute temporal resolution. The time period analyzed was from January to July 1999. A power-law event-size distribution was obtained for s between about 0.01 mm and 30 mm, with an exponent $\tau_s \simeq 1.4$. Dry-spell durations also seemed to follow a power-law distribution between 5 min and 4 days (roughly), with an exponent $\tau_q \simeq 1.4$, but superimposed to a daily peak. For the event-duration distribution the behavior was not so clear, although a power law with an exponent $\tau_d \simeq 1.6$ could be fit to the data. In any case, the clean power-law behavior obtained for the distributions of event sizes allowed to establish a patent parallelism between rainfall and SOC phenomena [19].

A radically different approach was followed by [20]. Instead of addressing their attention to the event-size distribution and looking for a power-law behavior (as in the overwhelming majority of SOC studies), they analyzed, from the Tropical Rainfall Measuring Mission, satellite microwave estimates of rain rate and vertically integrated (i.e., column) water vapour content in grid points covering the tropical oceans (with a

0.25° spatial resolution in latitude and longitude). The results were not only interesting as a support of SOC ideas but also for the characterization of rainfall phenomena and the problem of atmospheric convection. They showed a relationship between the two variables in the form of a sharp increase of the rain rate when a threshold value of the water vapor was reached, analogous to what is obtained in critical phase transitions. Moreover, these authors also demonstrated that most of the time the state of the system was close to the transition point (i.e., most of the measurements of the water vapor correspond to values near the critical one), providing perhaps the first direct observational support of the applicability of SOC theory to the natural world. Further, they connected these ideas with the classical concept of atmospheric quasi-equilibrium proposed by Arakawa and Schubert around 35 years ago [21].

In summary, the question of the existence of SOC in rainfall is far from being totally solved. Power-law size distributions allow a connection to be established: if SOC systems show distributions that are power law, and the system under study displays a power-law distribution, there exists the possibility that the system is a SOC system, although alternative mechanisms could explain the power law [3, 22]. In any case, the work of [16] resulted inconclusive in terms of establishing a link between rainfall and SOC, whereas the positive power-law findings of [17] could be considered somewhat "incidental", as it was based in a single dataset from a mid-latitude region.

In contrast, the key findings of Peters and Neelin suggest the existence of an attractive critical point in the rainfall transition over the tropical oceans, but curiously, the most common "test" for SOC, the construction of the event-size distribution, has barely been applied to tropical precipitation records (but see [23]). The goal of this paper is to contribute to extend the evidence for SOC in rainfall, studying a climatology that can be considered as a link between the Baltic-sea case analyzed by Peters *et al.* and the tropical oceans of Peters and Neelin. With this purpose, we perform an in-depth analysis of local (i.e., zero-dimensional) rainfall records in Catalonia, a representative region of the Northwestern Mediterranean. Indeed, we can view rainfall there as something in between the Baltic rain and the tropical convection, dominated by frontal systems during the Winter and mainly of convective origin in the Summer. Additionally, as a by-product of our study, we obtain a complete characterization of rain in the Catalonia region, which we consider generalizable to the Northwestern Mediterranean. A much broader study, covering very different climates and using rain data with higher resolution will be presented in [24], in order to verify the universality of rain-event statistics.

Note that the presence of SOC in rainfall has important consequences for the risks posed by this natural phenomenon. If there is not a characteristic rain-event size, then there is neither a definite separation nor a fundamental difference between the smallest harmless rains and the most hazardous storms. Further, the critical evolution of the rain events suggests that, at a given instant, it is equally likely that the rain rate intensifies or decreases, the outcome depending on a myriad of uncontrollable details, which makes detailed prediction unattainable in practice [25]. Our findings imply that this is the case for Mediterranean storms.

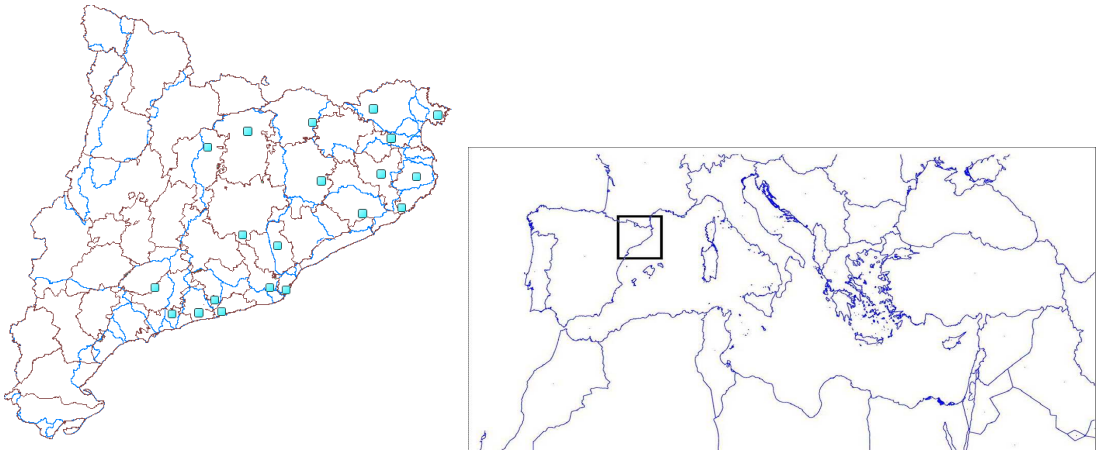

FIGURE 1. Map showing the position of the rain gauges analyzed across Catalonia. The location of the region in the NW of the Mediterranean is also shown. (Coast lines and old political borders taken from `http://rimmer.ngdc.noaa.gov/coast`.)

2. DATA

We have analyzed 20 stations in Catalonia (NE Spain) from the database maintained by the Agència Catalana de l'Aigua (ACA, `http://aca-web.gencat.cat/aca`). These data come from a network of rain gauges, called SICAT (Sistema Integral del Cicle de l'Aigua al Territori, formerly SAIH, Sistema Automàtic d'Informació Hidrològica); part of the stations belong to the ACA and the rest to the Servei Meteorològic de Catalunya, and they are used to monitor the state of the inland drainage basins of this region. The inland basins are those comprising the rivers which are born and die in the Catalan territory [26]. The corresponding sites are listed in Table 1, together with their latitude and longitude; a map is also provided in Fig. 1. All datasets cover a time period starting on January 1st, 2000, at 0:00, and ending either on June 30th or on July 1st, 2009 (spanning roughly 9.5 years), except the Cap de Creus one, which ends on June 19th, 2009 (this is just a 0.35 % relative difference in record length). The same database, although for a different time period, was also used in [26].

In all the stations, rain is measured by the same weighing precipitation gauge, the device called *Pluvio* from OTT (`http://www.ott-hydrometry.de`), either with a capacity of 250 or 1000 mm and working through the balance principle. It measures both liquid or/and solid precipitation. The precipitation rate is recorded in intervals of $\Delta t = 5$ min, with a resolution of 1.2 mm/hour (which corresponds to 0.1 mm in 5 min). This precipitation rate can be converted into an energy flux through the latent heat of condensation of water, which yields 1 mm/hour $\simeq$ 690 W/m^2 (this is about half the value of the solar constant). An example of a complete record is provided in Fig. 2 for the site of Muga.

TABLE 1. Characteristics of all the sites for the 9-year period 2000-2008. Every site is named by the corresponding river basin or subbasin, the municipality is included only in ambiguous cases. Ll. stands for Llobregat river. f_M is the fraction of missing records (time missing divided by total time); f_D is the fraction of discarded times; f_r is the fraction of rainy time (time with $r > c$ divided by total undiscarded time, for a time resolution $\Delta t = 5$ min); a. rate is the annual rain rate, calculated only over undiscarded times; c. rate is the rain rate conditioned to rain, i.e., calculated over the (undiscarded) rainy time; N_s is the number of rain events and N_q the number of dry spells; the rest of symbols are explained in the text. The differences between N_s and N_q are due to the missing records. Sites are ordered by increasing annual rate. The table shows a positive correlation between f_r, the annual rate, N_s and N_q, and that these variables are negatively correlated with $\langle q \rangle$ and $\langle q^2 \rangle / \langle q \rangle$. In contrast, the rate conditioned to rain is roughly constant, taking values between 3.3 and 3.8 mm/hour.

site	longitude E	latitude N	f_M %	f_D %	f_r %	a. rate mm/yr	c. rate mm/h	N_s	N_q	$\langle s \rangle$ mm	$\frac{\langle s^2 \rangle}{\langle s \rangle}$ mm	$\langle d \rangle$ min	$\frac{\langle d^2 \rangle}{\langle d \rangle}$ min	$\langle q \rangle$ min	$\frac{\langle q^2 \rangle}{\langle q \rangle}$ min
1 Gaià	1° 20' 18"	41° 14' 09"	0.08	3.71	1.6	470.9	3.3	5021	5014	0.81	11.7	14.9	92.4	894.	17958.
2 Foix	1° 39' 15"	41° 15' 26"	0.07	3.38	1.6	500.6	3.6	4850	4844	0.90	14.8	15.0	73.1	929.	17823.
3 Baix Ll. S.J. Despí	2° 02' 52"	41° 21' 13"	0.07	2.28	1.7	505.8	3.3	5374	5369	0.83	13.5	15.0	71.6	847.	16723.
4 Garraf	1° 41' 39"	41° 13' 55"	0.09	3.30	1.6	507.8	3.7	4722	4716	0.94	15.2	15.2	68.1	956.	15485.
5 Baix Ll. Castellbell	1° 51' 34"	41° 38' 54"	0.06	2.81	1.7	510.7	3.4	4950	4947	0.90	12.4	15.8	77.2	914.	16060.
6 Francolí	1° 10' 51"	41° 21' 60"	0.44	13.37	1.8	528.2	3.4	4539	4540	0.91	11.3	16.1	78.6	887.	13627.
7 Besòs Barcelona	2° 12' 06"	41° 27' 09"	0.15	4.17	1.7	531.8	3.5	4808	4803	0.95	12.1	16.2	70.5	928.	18617.
8 Riera de La Bisbal	1° 32' 15"	41° 12' 53"	0.07	3.66	1.6	540.0	3.8	4730	4724	0.99	13.8	15.8	75.2	950.	18334.
9 Besòs Castellar	2° 04' 57"	41° 36' 37"	4.34	13.59	2.0	633.3	3.6	4918	4970	1.00	11.6	16.9	79.5	806.	17276.
10 Ll. Cardener	1° 35' 14"	42° 06' 14"	0.07	3.33	2.1	652.4	3.5	6204	6197	0.92	10.0	15.7	68.6	723.	13986.
11 Ridaura	2° 58' 49"	41° 49' 12"	0.12	2.41	2.0	674.2	3.8	5780	5774	1.02	19.3	16.1	87.7	784.	12702.
12 Daró	3° 02' 22"	41° 57' 59"	0.06	2.09	2.2	684.5	3.6	5553	5547	1.09	16.9	18.0	109.2	818.	14054.
13 Tordera	2° 40' 14"	41° 44' 50"	0.08	2.04	2.3	688.8	3.4	7980	7977	0.76	14.1	13.6	93.2	568.	11999.
14 Baix Ter	2° 49' 32"	41° 58' 37"	0.07	2.71	2.3	710.2	3.6	6042	6036	1.03	16.4	17.4	104.7	746.	12949.
15 Cap de Creus	3° 07' 35"	42° 25' 40"	0.07	2.92	2.3	741.5	3.7	5962	5955	1.09	22.6	17.7	123.3	754.	13864.
16 Alt Llobregat	1° 52' 15"	42° 12' 58"	3.12	5.82	2.6	742.8	3.3	6970	6988	0.90	11.0	16.7	87.9	621.	10675.
17 Muga	2° 50' 10"	42° 20' 42"	0.06	2.56	2.4	749.3	3.6	6462	6457	1.02	31.5	16.9	119.4	698.	11415.
18 Alt Ter Sau	2° 24' 53"	41° 58' 14"	0.08	2.43	2.5	772.1	3.6	6966	6961	0.97	15.2	16.3	112.6	647.	11292.
19 Fluvià	2° 57' 20"	42° 09' 20"	3.09	4.74	2.3	772.4	3.8	6287	6319	1.05	19.0	16.7	99.6	697.	8881.
20 Alt Ter S. Joan	2° 14' 38"	42° 13' 25"	0.07	1.98	2.8	795.1	3.3	8333	8327	0.84	11.4	15.5	91.1	542.	7260.

In order to make the datasets more manageable, zero-rain rates are reported only every hour. This leads us to infer that time intervals larger than 1 hour have to be considered as operational errors. The ratio of these missing times to the total time covered in the record is denoted as f_M in Table 1, where it can be seen that this ratio is usually below 0.1 %. However, there are 3 cases in which its value is around 3 or 4 %. Other quantities reported in the table are the fraction of time corresponding to

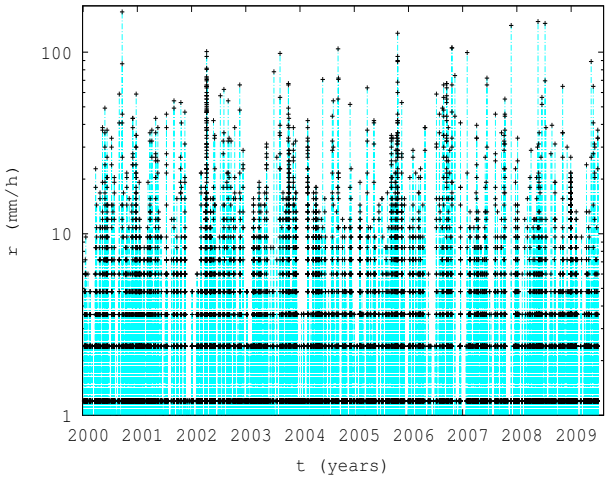

FIGURE 2. Evolution of the rate in the Muga site for the 9.5 years spanned by the record.

rain, f_r, the annual mean rate, and the mean rate conditioned to rain periods. Note that for a fractal point process a quantity as f_r only makes sense for a concrete time resolution, in our case, $\Delta t = 5$ min.

3. Analysis and Results

3.1. **Rain events and dry spells.** As we have mentioned in the first section, the key of our analysis is the rain event [16, 17]. If $r(t)$ denotes the rain rate at discrete time t (in intervals of 5 minutes in our case), a rain event is defined by the sequence of rates $\{r(t_n), r(t_{n+1}), \dots r(t_m)\}$ such that $r(t_i) > c$ for $i = n, n+1, \dots m$, but with $r(t_i) \leq c$ for $i = n-1$ and $i = m+1$. In words: a rain event starts when the threshold c is surpassed, all the rates in the event are above the threshold, and it ends when the rate crosses the threshold from above. In this paper we have considered $c = 0$, which, due to the resolution of the record, is equivalent to take $c \to 1.2^-$ mm/hour (where the superscript means that we are just below the value 1.2).

A quantity of interest is the duration d of the event, which is the time period covered by the sequence of above-threshold rates, i.e., $d \equiv t_m - t_n + \Delta t$; note that this is a multiple of $\Delta t = 5$ min. Even more relevant it is to consider the size of the event, which is defined as the total rain collected during the event,

$$s \equiv \sum_{i=n}^{m} r(t_i)\Delta t \simeq \int_{t_n}^{t_m} r(t)dt;$$

it is measured in mm and it is always a multiple of 0.1 mm (1.2 mm/hour $\times$ 5 min). The event size is proportional, through the latent heat of condensation, to the energy

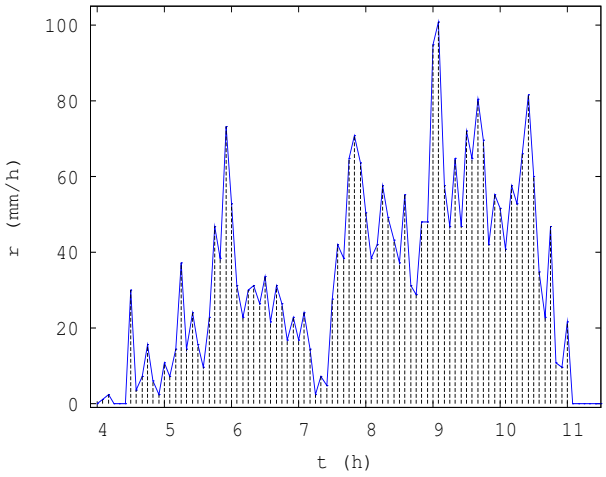

FIGURE 3. Time evolution of the rate of the rain event with the largest size in the Muga site. This event took place on April 11, 2002, and is also the largest (in size) of all sites, with $s = 248.7$ mm. Time refers to hours since midnight. A very small rain event is also present at the beginning, with $s = 0.3$ mm and separated to the main event by a dry spell of duration $q = 15$ min.

released by the event per unit area, with 1 mm $\simeq$ 2500 kJ/m^2 [24], and can be considered a measure of energy dissipation, as is done for SOC systems. Figure 3 shows as an illustration the evolution of the rate for the largest event in the record, which happens at the Muga site, whereas Fig. 4(a) displays the sequence of all events in the same site. Figure 4(b) shows the size of all events in Muga as a function of their duration, with considerable resemblance to [27]. Further, the dry spells are the periods between consecutive rain events (then, they verify $r(t) \leq c$). If the last record of an event is at t_m and the next event starts at the interval $t = t_p$, the dry-spell duration is $q \equiv t_p - t_m - \Delta t$, which is also a multiple of 5 min.

When a rain event, or a dry spell, is interrupted due to missing data, we discard that event or dry spell, and count the recorded duration as discarded time; the fraction of these times in the record appears in Table 1, under the symbol f_D. Although in some cases the duration of the interrupted event or dry spell can be bounded from below or from above, we have not attempted that estimation.

3.2. **Rain-event and dry-spell probability densities.** Due to the enormous variability of the 3 quantities just defined, the most informative approach is to work with their probability distributions. Taking the size as an example, its probability density $P_s(s)$ is defined as the probability that the size is between s and $s + ds$ divided by ds, with $ds \to 0$. Then, $\int_0^\infty P_s(s)ds = 1$. This implicitly assumes that s is considered as a continuous variable (but see below). Note that the annual number densities

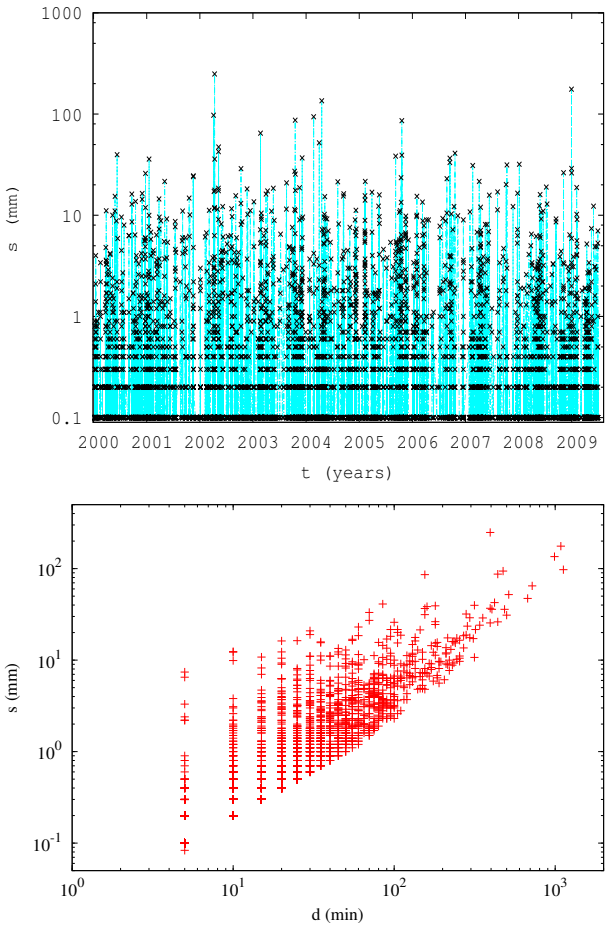

FIGURE 4. (a) Size of all rain events versus their occurrence time in the Muga site. (b) Size of all rain events as a function of their duration in the same site. Note that the event with the largest size is not the longest one.

[17, 18, 19] are trivially recovered multiplying the probability densities by the total number of events and dividing by total time.

In practice, the estimation of the density from data is performed taking a value of ds large enough to guarantee statistical significance, and then compute $P_s(s)$ as $n(s)/(N_s\Delta)$, where $n(s)$ is the number of events with size in the range between s and $s+ds$, N_s the total number of events, and Δ is defined as $\Delta = R_s(\lfloor (s+ds)/R_s \rfloor - \lfloor s/R_s \rfloor)$, with R_s the resolution of s, i.e. $R_s = 0.1$ mm, and $\lfloor x \rfloor$ the integer part of x (but note that high resolution means low R_s). So, Δ/R_s is the number of possible different values of the variable in the interval considered. Notice that using Δ instead of ds in the denominator of the estimation of $P_s(s)$ allows one to take into account the

discreteness of s. If R_s tended to zero, then $\Delta \to ds$ and the discreteness effects would become irrelevant.

How large does ds have to be to guarantee the statistical significance of the estimation of $P_s(s)$? Working with long-tailed distributions (where the variable covers a broad range of scales) a very useful procedure is to take a width of the interval ds that is not the same for all s, but that is proportional to the scale, as $[s, s+ds) = [s_o, bs_o)$, $[bs_o, b^2 s_o)$, ... $[b^k s_o, b^{k+1} s_o)$, i.e., $ds = (b-1)s$ (with $b > 1$). Given a value of s, the corresponding value of k that associates s with its bin is given by $k = \lfloor \log_b(s/s_o) \rfloor$. Correspondingly, the optimum choice to assign a point to the interval $[s, s+ds)$ is given by the value $\sqrt{b}s$. This procedure is referred to as logarithmic binning, because the intervals appear with fixed width in logarithmic scale [28]. In this paper we have generally taken $b \simeq 1.58$, in such a way that $b^5 = 10$, providing 5 bins per order of magnitude.

As the distributions are estimated from a finite number of data, they display statistical fluctuations. The uncertainty characterizing these fluctuations is simply related to the density by

$$\frac{\sigma_D(s)}{P_s(s)} \simeq \frac{1}{\sqrt{n(s)}},$$

where $\sigma_D(s)$ is the standard deviation of $P_s(s)$ (do not confound with the standard deviation of s). This is so because $n(s)$ can be considered a binomial variable [29], and then, the ratio between its standard deviation and mean fulfills $\sigma_n(s)/\langle n(s) \rangle = \sqrt{N_s p(1-p)}/(N_s p) \simeq \sqrt{(1-p)/n(s)} \simeq 1/\sqrt{n(s)}$, with $n(s) \simeq pN_s$ and $p \ll 1$. As $P_s(s)$ is proportional to $n(s)$, the same relation holds for its relative uncertainty.

The results for the probability densities $P_s(s)$, $P_d(d)$, and $P_q(q)$ of all the sites under study are shown in Fig. 5. In all cases the distributions show a very clear behavior, monotonically decreasing and covering a broad range of values. However, to the naked eye, the power-law behavior necessary for SOC is not clearly apparent, in general (remember that a power law appears as a straight line in a double logarithmic plot, i.e., $\log P_s(s) = -\tau_s \log s + \text{constant}$). Only the distribution of dry spells, $P_q(q)$, seems to be clearly linear between certain values of q. Moreover, these are the broadest distributions, covering a range of more than 4 orders of magnitude, from 5 min to about a couple of months. In addition, a daily peak seems to be present in some sites (1 day = 1440 min), as in [17]. In the opposite side we find the distributions of durations, $P_d(d)$, whose range is the shortest, from 5 min to about 1 day (two and a half decades), and for which no straight line is visible in the plot; rather, the distributions appear as convex. The size distributions $P_s(s)$ are somehow in between, defined for about 3 orders of magnitude (from 0.1 to 200 mm roughly) and perhaps with a short range of power-law behavior.

3.3. **Fitting and testing power laws.** A quantitative method can put more rigor into these observations. The idea is based on the recipe proposed by [30], but generalized to our problem. Essentially, an objective procedure is required in order to find the optimum range in which a power law may hold. Taking again the event size for

illustration, we report the power-law exponent fit between the values of $s_{\min}$ and $s_{\max}$ which yield the maximum number of data in that range but with a $p-$value greater than 10%. The method is described in detail in [24], but we summarize it in the next paragraphs.

For a given value of the pair $s_{\min}$ and $s_{\max}$, the maximum-likelihood (ML) power-law exponent is estimated for the events whose size lies in that range. This exponent yields a fit of the distribution, and the goodness of such a fit is evaluated by means of the Kolmogorov-Smirnov (KS) test [31]. The purpose is to get a $p-$value, which is the probability that the KS test gives a distance between true power law data and its fit larger than the distance obtained between the empirical data and its fit.

For instance, $p = 20\%$ would mean that truly power-law distributed data were closer than the empirical data to their respective fits in 80% of the cases, but in the rest 20% of the cases a true power law were at a larger distance than the empirical data. So, in such a case the KS distance turns out to be somewhat large, but not large enough to reject that the data follow a power law with the ML exponent.

As in the case in which some parameter is estimated from the data there is no closed formula to calculate the $p-$value, we perform Monte Carlo simulations in order to compute the statistics of the Kolmogorov-Smirnov distance and from there the $p-$value. In this way, for each $s_{\min}$ and $s_{\max}$ we get a number of data in that range and a $p-$value. We look for the values of the extremes ($s_{\min}$ and $s_{\max}$) which maximize the number of data in between but with the restriction that the $p-$value has to be greater than 10% (this threshold is arbitrary, but the conclusions do not change if it is moved). The maximization is performed sweeping 100 values of $s_{\min}$ and 100 values of $s_{\max}$, in log-scale, in such a way that all possible ranges (within this log-resolution) are taken into account. We have to remark that, in contrast with [24], we have considered always discrete probability distributions, both in the ML fit and in the simulations. Notice also that the method is not based on the estimation of the probability densities shown in the previous subsections.

The results of this method are in agreement with the visual conclusions obtained in the previous subsection, as can be seen in Table 2. Starting with the size statistics, 13 out of the 20 sites yield reasonable results, with an exponent τ_s between 1.43 and 1.54 over a logarithmic range $s_{\max}/s_{\min}$ from 12 to more than 200. For the rest of the sites, the range is too short (less than one decade). In the application of the algorithm, it has been necessary to restrict the value of $s_{\min}$ to be $s_{\min} \geq 0.2$ mm; otherwise, as the distributions have a concave shape (in logscale) close to the origin (which means that there are many more events in that scale than at larger scales), the algorithm (which maximizes the number of data in a given range) prefers a short range with many data close to the origin than a larger range with less data away from the origin. Perhaps a variation of the algorithm in which the quantity that is maximized is the logarithmic range would not need this restriction.

For the distribution of durations the results are worse, as expected (worse in the sense that the power-law fit is worse than in the previous case). Only 4 sites do not give totally unacceptable results, with τ_d ranging from 1.66 to 1.74 and d_{max}/d_{min} from

6 to 12. The other sites yield too short ranges for the power law be of any relevance. The situation is analogous to the case of the distribution of sizes, but the resulting ranges are much shorter here [24]. Notice that the excess of events with $d = 5$ min, eliminated from the fits imposing $d_{min} \geq 10$ min, has no counterpart in the value of the smallest rate (not shown), and therefore, this extra number of events is probably due to problems in the time resolution of the data.

Considerably better are the results for the dry spells. 16 sites give consistent results, with τ_q from 1.45 to 1.55 in a range q_{max}/q_{min} from 30 to almost 300. It is noticeable that in these cases q_{max} is always below 1 day. Perhaps, the removal by hand of dry spells around that value could enlarge a little the power-law range. In the rest of sites, either the range is comparatively too short (for example, for the Gaià site, the power-law behavior of $P_q(q)$ is interrupted at around $q = 100$ min), or the algorithm has a tendency to include the bump the distributions show between the daily peak (q beyond 1000 min) and the tail. This makes the value of the exponent smaller.

In summary, the best power laws for the distributions of durations are too short to be relevant, and the fits for the sizes are in the limit of what is acceptable or not (some cases are clear and some other not). Only the distributions of dry spells give really good power laws (with $\tau_q = 1.50 \pm 0.05$, and for more than two decades in 6 sites).

3.4. **Non-parametric scaling.** Nevertheless, the fact that a power-law behavior does not exist over a broad range of values does not rule out the existence of SOC [4]. In fact, the fulfillment of a power-law distribution in the form of Eq. (1) is only valid when finite-size effects are "small", which only happens for large enough systems. In general, when these effects are taken into account, SOC behavior leads to distributions of the form [4, 24]

$$P_s(s) = s^{-\tau_s}\mathcal{G}_s(s/s_\xi) \quad \text{for } s > s_l, \tag{2}$$

where $\mathcal{G}_s(x)$ is a scaling function that is essentially constant for $x < 1$ and decays fast for $x > 1$, accounting in this way for the finite-size effects when s is above the crossover value s_ξ; the size s_l is just a lower cutoff limiting the validity of this description. Notice that for a power-law behavior to hold over an appreciable range, it is necessary that the scales given by s_l and s_ξ are well separated, i.e., $s_l \ll s_\xi$. As s_ξ increases with system size, typically as $s_\xi \propto L^{D_s}$ (with D_s the so-called avalanche dimension, or event-size dimension), the power-law condition (1) can only be fulfilled for large enough system sizes.

However, it is not clear what the system size L is for rainfall. May it be the vertical extension of the clouds, or the depth of the troposphere? In any case, we do not need to bother about its definition since, whatever it is, it is not accessible to us (remember that all our data are just local rain rates). Nevertheless, the scaling ansatz (2) still can be checked from data. First, notice that the ansatz implies that the $k-$order moment of s scale with L as

$$\langle s^k \rangle \propto L^{D_s(k+1-\tau_s)} \quad \text{for } 1 < \tau_s < k+1, \tag{3}$$

TABLE 2. Results of the power-law fitting and goodness-of-fit tests applied to event sizes, event durations, and drought durations, for the period of 9 and a half years specified in the main text. The table displays the minimum and maximum fitting range, the ratio of these values (logarithmic range), total number of events, number of events in fitting range ($\bar{N}_s$, $\bar{N}_d$, and $\bar{N}_q$, for s, d, and q, respectively), and the power-law exponent with its uncertainty (one standard deviation) calculated as stated by [32] and displayed between parenthesis as the variation of the last digit. All the fits have a $p-$value larger than 10 %. The results of [18], labeled as ChP, are also included, the fitting ranges are estimated visually from their plots.

site	s_{min} mm	s_{max} mm	$\frac{s_{max}}{s_{min}}$	N_s	$\bar{N}_s$	τ_s	d_{min} min	d_{max} min	$\frac{d_{max}}{d_{min}}$	$\bar{N}_d$	τ_d	q_{min} min	q_{max} min	$\frac{q_{max}}{q_{min}}$	N_q	$\bar{N}_q$	τ_q
1	0.2	36.1	180.5	5393	1886	1.54(2)	10	100	10.0	1668	1.67(4)	95	740	7.8	5387	743	1.75(7)
2	0.2	0.9	4.5	5236	1323	1.64(6)	10	40	4.0	1581	1.60(6)	5	1365	273.0	5231	4729	1.46(1)
3	0.2	31.1	155.5	5749	2111	1.53(2)	10	60	6.0	1726	1.66(5)	10	800	80.0	5745	3207	1.53(2)
4	0.2	2.4	12.0	5108	1745	1.43(3)	10	35	3.5	1564	1.41(7)	5	980	196.0	5103	4520	1.47(1)
5	0.2	28.0	140.0	5289	2106	1.52(2)	10	35	3.5	1530	1.58(7)	20	945	47.3	5287	1706	1.45(2)
6	0.2	13.6	68.0	4924	1969	1.49(2)	10	35	3.5	1441	1.59(7)	20	625	31.3	4926	1537	1.47(3)
7	0.2	21.1	105.5	5219	2234	1.51(2)	10	35	3.5	1621	1.51(7)	5	1280	256.0	5215	4734	1.51(1)
8	0.2	42.6	213.0	5112	2047	1.53(2)	10	40	4.0	1567	1.55(6)	15	975	65.0	5107	2098	1.50(2)
9	0.2	1.0	5.0	5366	1459	1.53(5)	10	40	4.0	1658	1.51(6)	10	900	90.0	5419	2889	1.55(2)
10	0.2	3.8	19.0	6691	2452	1.51(2)	10	35	3.5	2066	1.57(6)	25	825	33.0	6685	1758	1.48(3)
11	0.2	13.0	65.0	6224	2373	1.49(2)	10	50	5.0	1932	1.56(5)	45	21075	468.3	6219	2005	1.24(1)
12	0.2	0.8	4.0	5967	1500	1.53(6)	10	40	4.0	1889	1.49(6)	5	1175	235.0	5961	5376	1.47(1)
13	0.3	20.0	66.7	8330	1853	1.45(2)	10	125	12.5	2288	1.74(3)	130	20600	158.5	8328	1501	1.27(2)
14	0.2	0.7	3.5	6525	1711	1.56(6)	10	50	5.0	2299	1.62(4)	5	1075	215.0	6520	5906	1.47(1)
15	0.3	1.1	3.7	6485	1102	1.39(7)	10	50	5.0	2095	1.64(5)	15	745	49.7	6479	2560	1.51(2)
16	0.2	0.7	3.5	7491	1852	1.59(5)	10	40	4.0	2385	1.59(5)	5	1070	214.0	7510	6789	1.50(1)
17	0.2	16.1	80.5	6962	2853	1.52(2)	10	35	3.5	2087	1.60(6)	10	685	68.5	6958	3719	1.52(1)
18	0.2	8.3	41.5	7511	2847	1.51(2)	10	35	3.5	2238	1.57(6)	20	620	31.0	7507	2302	1.53(2)
19	0.2	19.9	99.5	6767	2742	1.47(2)	10	35	3.5	1958	1.60(6)	50	1085	21.7	6800	1378	1.26(3)
20	0.2	0.7	3.5	9012	2047	1.69(5)	10	85	8.5	2972	1.66(3)	15	515	34.3	9007	3367	1.50(2)
ChP	0.01	30	300	–	–	1.4	10	300	30	–	1.6	5	*6000	1200	–	–	1.4

* Disregarding the daily peak.

if $s_l \ll s_\xi$, see [4]. Second, Eq. (2) can be written in a slightly different form, as a scaling law,

$$P_s(s) = L^{-D_s\tau_s}\mathcal{F}_s(s/L^{D_s}) \quad \text{for } s > s_l, \tag{4}$$

where the new scaling function $\mathcal{F}_s(x)$ is defined as $\mathcal{F}_s(x) \equiv x^{-\tau_s}\mathcal{G}_s(x/a)$ (a is the constant of proportionality between s_ξ and L^{D_s}). This form of $P_s(s)$ (in fact, $P_s(s, L)$), with an arbitrary $\mathcal{F}$, is the well-known scale-invariance condition [4, 6]. Changes of scale (linear transformations) in s and L may leave the shape of the function $P_s(s, L)$ unchanged (this is what scale invariance means, power laws are just a particular case).

Substituting $L^{D_s} \propto \langle s^2 \rangle / \langle s \rangle$ and $L^{D_s \tau_s} \propto L^{2D_s} / \langle s \rangle \propto \langle s^2 \rangle^2 / \langle s \rangle^3$ (from the scaling of $\langle s^k \rangle$, assuming $\tau_s < 2$) into Eq. (4) leads to

$$P_s(s) = \langle s \rangle^3 \langle s^2 \rangle^{-2} \tilde{\mathcal{F}}_s(s \langle s \rangle / \langle s^2 \rangle) \tag{5}$$

where $\tilde{\mathcal{F}}_s(x)$ is essentially the scaling function $\mathcal{F}_s(x)$, absorbing the proportionality constants. Therefore, if scaling holds, a plot of $\langle s^2 \rangle^2 P_s(s) / \langle s \rangle^3$ versus $s \langle s \rangle / \langle s^2 \rangle$ for all the sites has to yield a collapse of the distributions into a single curve, which draws $\tilde{\mathcal{F}}_s(x)$ (a similar procedure is outlined in [33]). In order to proceed, the mean and the quadratic mean, $\langle s \rangle$ and $\langle s^2 \rangle$, can be easily estimated from data. These values, and the corresponding ones for d and q are displayed for all sites in Table 1.

The outcome for $P_s(s)$, $P_d(d)$, and $P_q(q)$ is shown in Fig. 6, with reasonable results, especially for the distribution of dry spells. In this case, the plot suggests that the scaling function $\mathcal{G}_q(x)$ has a maximum around $x \simeq 1$, but this does not invalidate our approach, which assumed constant $\mathcal{G}_q(x)$ for small x and a fast decay for large x.

Note that the quotient $\langle s^2 \rangle / \langle s \rangle$ gives the scale for the crossover value s_ξ (as $s_\xi \propto \langle s^2 \rangle / \langle s \rangle$, with a constant of proportionality that depends on the scaling function $\mathcal{G}_s$ and on s_l / s_ξ), and therefore it is the ratio of the second moment to the mean and not the mean which describes the scaling behavior of the distribution. For the case of event sizes, we get values of $\langle s^2 \rangle / \langle s \rangle$ between 10 and 30 mm (see Table 1), and therefore the condition $s_l \ll s_\xi$ is very well fulfilled (assuming that the moment ratio $\langle s^2 \rangle / \langle s \rangle$ is of the same order as s_ξ), which is a test for the consistency of our approach. For dry spells $\langle q^2 \rangle / \langle q \rangle$ is between 5 and 13 days, which is even better for the applicability of the scaling analysis. The case of the event durations is somewhat "critical", with $\langle d^2 \rangle / \langle d \rangle$ between 70 and 120 min, which yields d_ξ / d_l in the range from 14 to 24. Nevertheless, we observe that the condition $s_l \ll s_\xi$ for the power law to show up is stronger than the same condition for the scaling analysis to be valid.

3.5. **Parametric scaling.** Further, a scaling ansatz as Eq. (2) or (4) allows an estimation of the exponent τ_s, even in the case in which a power law cannot be fit to the data. From the scaling of the moments of s we get, taking $k = 1$, $L^{D_s} \propto \langle s \rangle^{1/(2-\tau_s)}$ and $L^{D_s \tau_s} \propto \langle s \rangle^{\tau_s/(2-\tau_s)}$ (again with $\tau_s < 2$); so, substituting into Eq. (4),

$$P_s(s) = \langle s \rangle^{-\tau_s/(2-\tau_s)} \hat{\mathcal{F}}_s(s / \langle s \rangle^{1/(2-\tau_s)}). \tag{6}$$

One only needs to find the value of τ_s that optimizes the collapse of all the distributions, i.e., that makes the previous equation valid, or at least as close to validity as possible.

We therefore need a measurement to quantify distance between rescaled distributions. In order to do that, we have chosen to work with the cumulative distribution function, $S_s(s) \equiv \int_s^\infty P_s(s')ds'$, rather than with the density (to be rigorous, $S_s(s)$ is the complementary of the cumulative distribution function, and is called survivor function or reliability function in some contexts). The reason to work with $S_s(s)$ is double: the estimation of the cumulative distribution function does not depend of an arbitrarily selected bin width ds [31], and it does not give equal weight to all scales

in the representation of the function (i.e., in the number of points that constitute the function). The scaling laws (4) and (6) turn out to be, then,

$$S_s(s) = L^{-D_s(\tau_s-1)}\mathcal{H}_s(s/L^{D_s}), \tag{7}$$

$$S_s(s) = \langle s\rangle^{-(\tau_s-1)/(2-\tau_s)}\,\hat{\mathcal{H}}_s(s/\langle s\rangle^{1/(2-\tau_s)}), \tag{8}$$

with $\mathcal{H}_s(x)$ and $\hat{\mathcal{H}}_s(x)$ the corresponding scaling functions.

The first step of the method of collapse is to merge all the pairs $\{s, S_s(s)\}_i$ into a unique rescaled function $\{x, y\}$. If $i = 1, \ldots, 20$ runs for all sites, and $j = 1, \ldots, M_s(i)$ for all the different values that the size of events takes on site i (note that $M_s(i) \leq N_s(i)$), then,

$$x_\ell(\tau) \equiv \log(s_{ji}/\langle s\rangle_i^{1/(2-\tau)}),$$
$$y_\ell(\tau) \equiv \log(S_{s\,i}(s_{ji})\,\langle s\rangle_i^{\tau/(2-\tau)}),$$

with s_{ji} the j-th value of the size in site i, $\langle s\rangle_i$ the mean on s in i, $S_{s\,i}(s_{ji})$ the cumulative distribution function in i, and τ a possible value of the exponent τ_s. The index ℓ labels the new function, from 1 to $\sum_{\forall i} M_s(i)$, in such a way that $x_\ell(\tau) \leq x_{\ell+1}(\tau)$; i.e., the pairs $x_\ell(\tau), y_\ell(\tau)$ are sorted by increasing x.

Then, we just compute

$$D(\tau) \equiv \sum_{\forall \ell} \left([x_\ell(\tau) - x_{\ell+1}(\tau)]^2 + [y_\ell(\tau) - y_{\ell+1}(\tau)]^2 \right), \tag{9}$$

which represents the sum of all Euclidean distances between the neighboring points in a (tentative) collapse plot in logarithmic scale. The value of τ which minimizes this function is identified with the exponent τ_s in Eq. (2). We have tested the algorithm applying it to SOC models whose exponents are well known, as the one in [34].

The results of this method applied to our datasets, not only for the size distributions but also to the distributions of d, are highly satisfactory. There is only one requirement: the removal of the first point in each distribution ($s = 0.1$ mm and $d = 5$ min), as with the ML fits. The exponents we find are $\tau_s = 1.52 \pm 0.12$ and $\tau_d = 1.69 \pm 0.01$, in agreement with the ones obtained by the power-law fitting method presented above, and the corresponding rescaled plots are shown in Fig. 7. The performance of the method is noteworthy, taking into account that the mean values of the distributions show little variation in most cases. In addition, the shape of the scaling function $\mathcal{G}_s$ can be obtained by plotting, as suggested by Eq. (2), $s^{\tau_s}P_s(s)$ versus $s/\langle s\rangle^{1/(2-\tau_s)}$, and the same for the other variable, d. Figure 8 displays what is obtained for each distribution.

4. Discussion and Conclusions

We have obtained evidence that rainfall in the Mediterranean region studied is compatible with self-organized criticality. For the distributions of rain-event sizes we get power-law exponents which are valid for at least one decade or even two in the majority of sites. For the rest of the sites the fitting range is too short, but this seems to be due to an inadequacy of the algorithm that looks for the optimum fitting range,

rather than to a real short power-law range in the data. The values of the exponents, $\tau_s \simeq 1.50 \pm 0.05$, are in reasonable agreement with the value reported for the Baltic sea in [17], $\tau_s \simeq 1.4$, more taking into account the different nature of the data analyzed and the disparate fitting procedures. So, we cannot rule out that the apparent agreement is a product of serendipity. For the distributions of event durations, the fitting ranges are much shorter, reaching in the best case one decade, although the obtained exponents in this case, $\tau_d \simeq 1.70 \pm 0.05$, are compatible too with the Baltic-sea result, $\tau_d \simeq 1.6$. Again, we suspect that the algorithm is the responsible for the failure in the other sites.

Nevertheless, for both observables (s and d) the range of the power laws seems rather limited. This is explained by the existence of finite size effects, as it is the case in other (self-organized and non-self-organized) critical phenomena. A finite-size analysis, in terms of combinations of powers of the moments of the distributions, supports this conclusion. The collapse of the distributions is a clear signature of scale-invariance: different sites share a common shape of the rain-event and dry-spell distributions, and the only difference is in the scale of those distributions, which depends on system size. In the ideal case, in an infinite system, the power laws could then be extended with no upper cutoff. Further, the collapse of the distributions allows one an independent estimate of the power-law exponents, in surprising agreement with the values obtained by the maximum-likelihood fit. Overall, these results are notable, in our opinion, as they support the idea that rainfall events follow a law of dissipation analogous to the Gutenberg-Richter law for earthquakes [35] and other natural hazards [12, 13, 14, 15, 36], which is the hallmark of SOC systems; up to now this evidence rested essentially on observations in a single place [17, 18, 19, 23].

However, comparison with the new results of [24] suggests that data resolution might play an important role in the determination of the exponents. With a minimum detection rate of 0.2 mm/hour and a time resolution $\Delta t = 1$ min it was found there that $\tau_s \simeq 1.18$, for several sites with disparate climatic characteristics, using essentially the same statistical techniques as in here. Better time resolution and lower detection threshold allow the detection of smaller events (a minimum s =0.003 mm in [24] versus 0.1 mm in our case), so it is possible that we cannot see the "true" asymptotic (small s) power-law regime and that, due to the presence of the tail, we get a larger value of the exponent. Another study with relatively poor resolution (0.1 mm/hour but $\Delta t = 1$hour) yielded distributions apparently compatible with $\tau_s \simeq 1.5$ for small s [37]. But one has to take also into account that a change in the detection threshold has a non-trivial repercussion in the size and duration of the events and the dry spells (an increase in the threshold can split one single event into two or more separate ones and vice versa). Therefore, we urge studies which explore the effects of resolution and detection-threshold value in high-resolution rain data. (Obviously, with poor resolution data the detection threshold cannot be decreased, but it can be artificially increased in very accurate data.)

On the other hand, the interpretation of the results for the distributions of dry spells is not so clear. These distributions yield by far the best power-law fits, with exponents in the range $\tau_q \simeq 1.50 \pm 0.05$ and in agreement with the previous result by [17].

However, power-law waiting times (or quiet times) between events is not a requirement for SOC; in fact, it was previously believed that SOC avalanches happen following a totally memoryless process, leading therefore to exponential distributions for the waiting times. This belief has been recently denied, see for instance [38], although a solution to this problem is not known yet. Nevertheless, in order to compare with SOC models, one would need to consider that in those cases the events are defined in a spatially extended system (in two or three dimensions), whereas our measurements are taken in a point of the system collecting only information on the vertical scale. This statement is general and should affect all the aspects of our research. Comparison with [24] shows that our value of the exponent is higher. But in this case, our power-law range is enough to guarantee that our estimation of the exponents are robust, and we can only explain the discrepancy with [24] by the non-trivial effect of the change in the detection thresholds.

In summary, we conclude that the statistics of rainfall events in the NW Mediterranean area studied is not essentially different to what is expected from the SOC paradigm and was confirmed essentially in one single place, up to now [24]. This concordance is not only qualitative but also quantitative, as only the mean rain rate is enough to characterize rain occurrence; in other words, the rain rate sets the scale around which all events are distributed following a common shape of the probability density. This seems to indicate that SOC observables do not allow to detect climatic different between regions (apart of the obvious ones given by annual rates), but shed light on universal properties of rainfall generation. The results of this paper are very valuable, taking into account that the ACA network was not designed for the study of the fine structure of rainfall; the database we use is probably in the limit of what can lead to detect the presence of SOC. This can motivate other researchers to look for SOC in intermediate-quality data, extending the evidence and the understanding of this complex phenomenon.

5. ACKNOWLEDGEMENTS

This work would not have been possible without the collaboration of the Agència Catalana de l'Aigua (ACA), which generously shared its rain data with us. We have benefited a lot from a long-term collaboration with Ole Peters, and are grateful also to R. Romero and A. Rosso, for addressing us towards the ACA data and an important reference [33], and to J. E. Llebot for providing support and encouragement. Thank you also to Joaquim Farguell from ACA. A.D. enjoys a Ph.D. grant of the Centre de Recerca Matemàtica. Her initial research was supported from the Explora-Ingenio 2010 project FIS2007-29088-E. Other grants related to this work are FIS2009-09508 and 2009SGR-164. A.C. is a participant of the CONSOLIDER i-MATH project.

References

[1] P. Bak. How Nature Works: The Science of Self-Organized Criticality. Copernicus, New York, 1996.

[2] H. J. Jensen. Self-Organized Criticality. Cambridge University Press, Cambridge, 1998.

[3] D. Sornette. Critical Phenomena in Natural Sciences. Springer, Berlin, 2nd edition, 2004.
[4] K. Christensen and N. R. Moloney. Complexity and Criticality. Imperial College Press, London, 2005.
[5] V. Frette, K. Christensen, A. Malthe-Sørenssen, J. Feder, T. Jøssang, and P. Meakin. Avalanche dynamics in a pile of rice. Nature, 379:49–52, 1996.
[6] A. Corral. Scaling and universality in the dynamics of seismic occurrence and beyond. In A. Carpinteri and G. Lacidogna, editors, Acoustic Emission and Critical Phenomena, pages 225–244. Taylor and Francis, London, 2008.
[7] C. Tang and P. Bak. Critical exponents and scaling relations for self-organized critical phenomena. Phys. Rev. Lett., 60:2347–2350, 1988.
[8] R. Dickman, A. Vespignani, and S. Zapperi. Self-organized criticality as an absorbing-state phase transition. Phys. Rev. E, 57:5095–5105, 1998.
[9] R. Dickman, M. A. Muñoz, A. Vespignani, and S. Zapperi. Paths to self-organized criticality. Braz. J. Phys., 30:27–41, 2000.
[10] P. Bak, C. Tang, and K. Wiesenfeld. Self-organized criticality: an explanation of $1/f$ noise. Phys. Rev. Lett., 59:381–384, 1987.
[11] A. Sornette and D. Sornette. Self-organized criticality and earthquakes. Europhys. Lett., 9:197–202, 1989.
[12] B. D. Malamud. Tails of natural hazards. Phys. World, 17 (8):31–35, 2004.
[13] F. Lahaie and J. R. Grasso. A fluid-rock interaction cellular automaton of volcano mechanics: Application to the Piton de la Fournaise. J. Geophys. Res., 103 B:9637–9650, 1998.
[14] B. D. Malamud, G. Morein, and D. L. Turcotte. Forest fires: An example of self-organized critical behavior. Science, 281:1840–1842, 1998.
[15] K. Sneppen, P. Bak, H. Flyvbjerg, and M. H. Jensen. Evolution as a self-organized critical phenomenon. Proc. Natl. Acad. Sci. USA, 92:5209–5213, 1995.
[16] R. F. S. Andrade, H. J. Schellnhuber, and M. Claussen. Analysis of rainfall records: possible relation to self-organized criticality. Physica A, 254:557–568, 1998.
[17] O. Peters, C. Hertlein, and K. Christensen. A complexity view of rainfall. Phys. Rev. Lett., 88:018701, 2002.
[18] O. Peters and K. Christensen. Rain: Relaxations in the sky. Phys. Rev. E, 66:036120, 2002.
[19] O. Peters and K. Christensen. Rain viewed as relaxational events. J. Hidrol., 328:46–55, 2006.
[20] O. Peters and J. D. Neelin. Critical phenomena in atmospheric precipitation. Nature Phys., 2:393–396, 2006.
[21] A. Arakawa and W. H. Schubert. Interaction of a cumulus cloud ensemble with the large-scale environment, part I. J. Atmos. Sci., 31:674–701, 1974.
[22] R. Dickman. Rain, power laws, and advection. Phys. Rev. Lett., 90:108701, 2003.
[23] J. D. Neelin, O. Peters, J. W.-B. Lin, K. Hales, and C. E. Holloway. Rethinking convective quasi-equilibrium: observational constraints for stochastic convective schemes in climate models. Phil. Trans. R. Soc. A, 366:2581–2604, 2008.
[24] O. Peters, A. Deluca, A. Corral, J. D. Neelin, and C. Holloway. Universality of rain event size distributions. J. Stat. Mech., to be submitted, 2010.
[25] E. Martin, A. Shreim, and M. Paczuski. Activity-dependent branching ratios in stocks, solar x-ray flux, and the Bak-Tang-Wiesenfeld sandpile model. Phys. Rev. E, 81:016109, 2010.
[26] M.-C. Llasat, M. Ceperuelo, and T. Rigo. Rainfall regionalization on the basis of the precipitation convective features using a raingauge network and weather radar observations. Atmos. Res., 83:415–426, 2007.
[27] L. Telesca, V. Lapenna, E. Scalcione, and D. Summa. Searching for time-scaling features in rainfall sequences. Chaos, Solitons and Fractals, 32:35–41, 2007.
[28] S. Hergarten. Self-Organized Criticality in Earth Systems. Springer, Berlin, 2002.

[29] R. von Mises. Mathematical Theory of Probability and Statistics. Academic Press, New York, 1964.
[30] A. Clauset, C. R. Shalizi, and M. E. J. Newman. Power-law distributions in empirical data. SIAM Rev., 51:661–703, 2009.
[31] W. H. Press, S. A. Teukolsky, W. T. Vetterling, and B. P. Flannery. Numerical Recipes in FORTRAN. Cambridge University Press, Cambridge, 2nd edition, 1992.
[32] H. Bauke. Parameter estimation for power-law distributions by maximum likelihood methods. Eur. Phys. J. B, 58:167–173, 2007.
[33] A. Rosso, P. Le Doussal, and K. J. Wiese. Avalanche-size distribution at the depinning transition: A numerical test of the theory. Phys. Rev. B, 80:144204, 2009.
[34] K. Christensen, A. Corral, V. Frette, J. Feder, and T. Jøssang. Tracer dispersion in a self-organized critical system. Phys. Rev. Lett., 77:107–110, 1996.
[35] H. Kanamori and E. E. Brodsky. The physics of earthquakes. Rep. Prog. Phys., 67:1429–1496, 2004.
[36] A. Corral, A. Ossó, and J. E. Llebot. Scaling of tropical-cyclone dissipation. Nature Phys., 6:693–696, 2010.
[37] A. P. García-Marín, F. J. Jiménez-Hornero, and J. L. Ayuso. Applying multifractality and the self-organized criticality theory to describe the temporal rainfall regimes in Andalusia (southern Spain). Hydrol. Process., 22:295–308, 2008.
[38] A. Corral. Comment on "Do earthquakes exhibit self-organized criticality?". Phys. Rev. Lett., 95:159801, 2005.

A. Deluca and A. Corral
Centre de Recerca Matemàtica
Edifici Cc, Campus Bellaterra
E-08193 Bellaterra (Barcelona), Spain

E-mail address: A. Corral, (acorral@crm.cat)

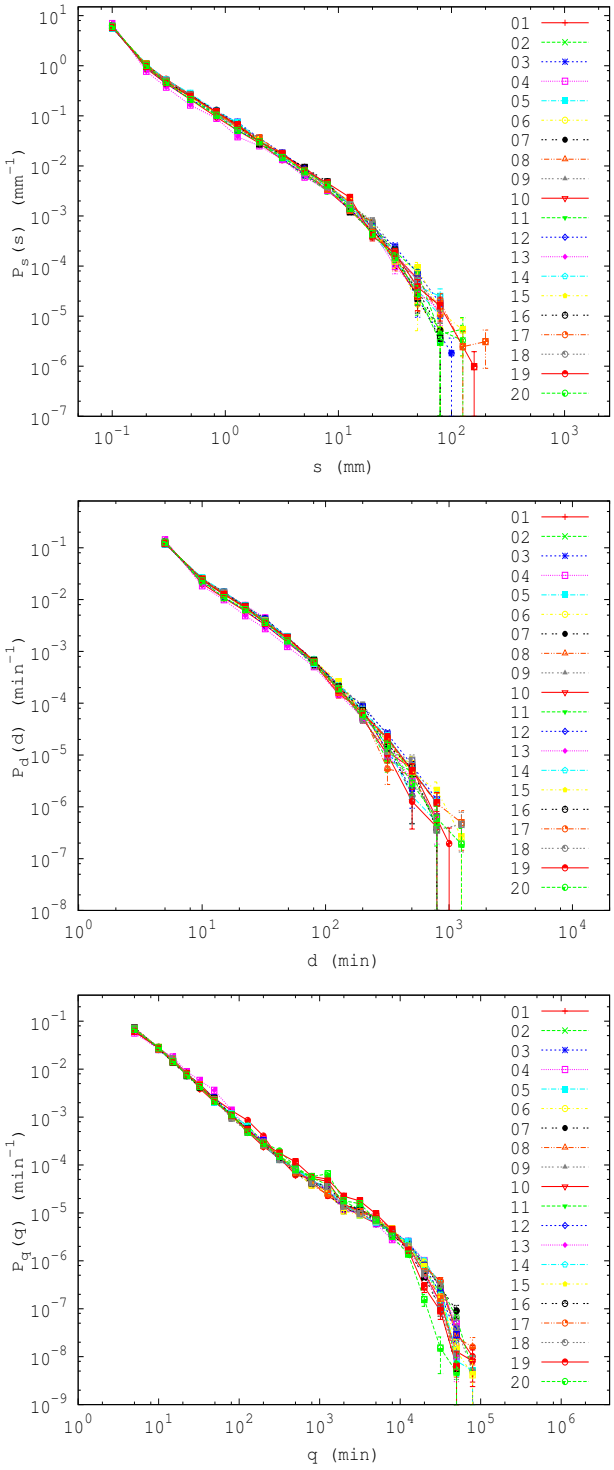

FIGURE 5. Event and dry-spell probability densities for all the sites for the whole time covered by the record. (a) Event-size distributions. (b) Event-duration distributions. (c) Dry-spell duration distributions. All sites show "similar" features.

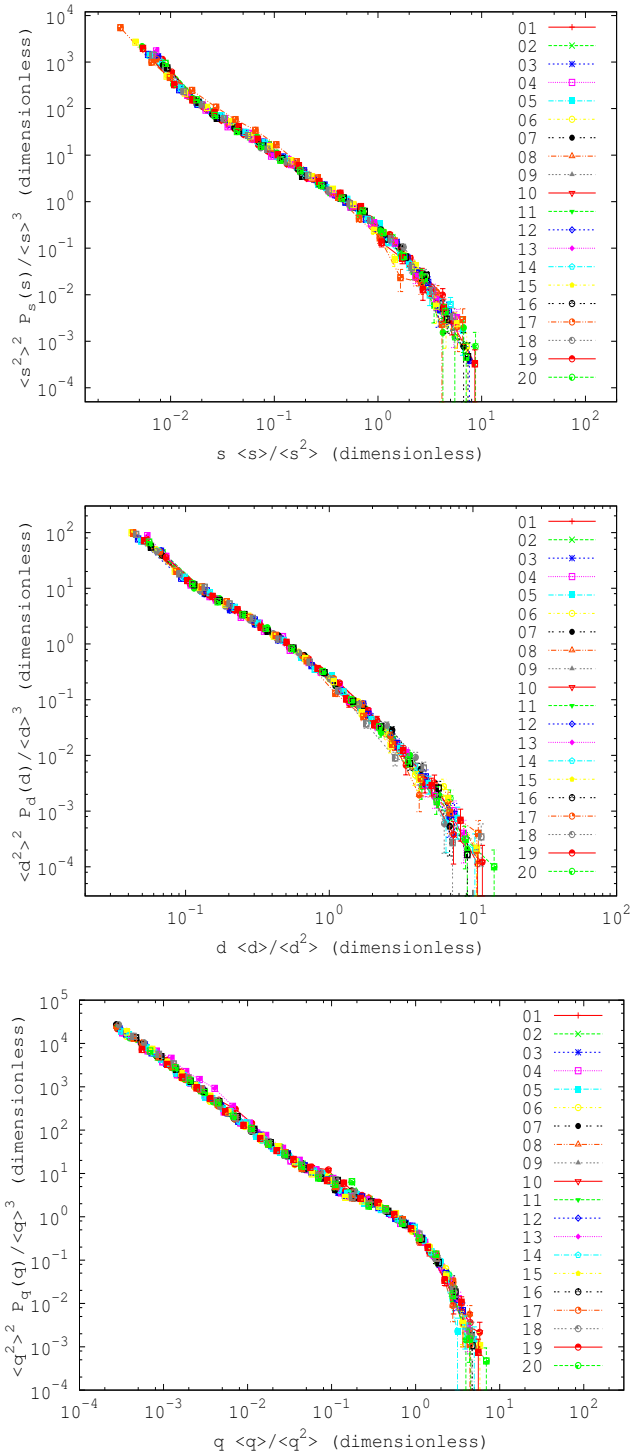

FIGURE 6. The same distributions of the previous plot but rescaled with a combination of their moments following Eq. (5).

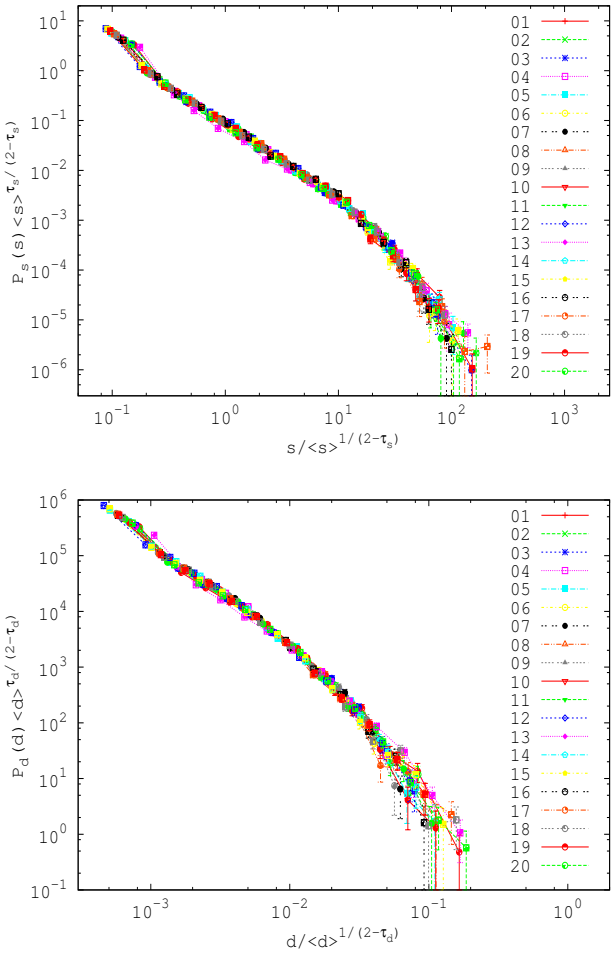

FIGURE 7. The distributions in Fig. 5 rescaled this time by a power of the mean, following Eq. (6), excluding dry-spell distributions. The values of the exponents are $\tau_s = 1.52$ and $\tau_d = 1.69$. Units are $\mathrm{mm}^{-(\tau_s-1)/(2-\tau_s)}$ for the abscissa and $\mathrm{mm}^{2(\tau_s-1)/(2-\tau_s)}$ for the ordinate in (a), and $\mathrm{min}^{-(\tau_d-1)/(2-\tau_d)}$ for the abscissa and $\mathrm{min}^{2(\tau_d-1)/(2-\tau_d)}$ for the ordinate in (b).

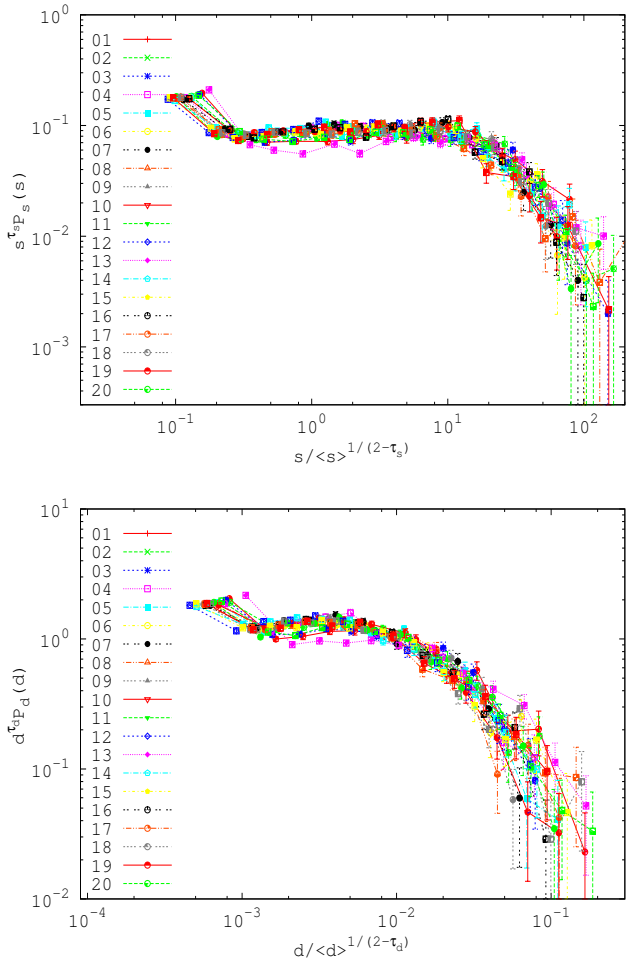

FIGURE 8. The rescaled distributions of the previous plot multiplied by s^{τ_s}, or d^{τ_d} in order to make apparent the shape of the scaling functions $\mathcal{G}_s$ and $\mathcal{G}_d$. Units in the abscissae are as in the previous plot, whereas in the ordinates these are mm^{τ_s-1} and min^{τ_d-1}.